16th World Conference on Earthquake, 16WCEE 2017

Santiago Chile, January 9th to 13th 2017

Paper N° 2634

Registration Code: S-I1461879556

NONLINEAR TIME-HISTORY ANALYSIS OF A BASE-ISOLATED RC BUILDING IN SHANGHAI FOUNDED ON SOFT SOIL

Weng Dagen(1), Li Tao(2), Bashar Alfarah(3), Francisco López-Almansa(4)

(1) *Tongji University, wdg@tongji.edu.cn*
(2) *Tongji University, ltlt52@gmail.com*
(3) *Technical University of Catalonia, bashar.alfarah@upc.edu*
(4) *Technical University of Catalonia, francesc.lopez-almansa@upc.edu*

Abstract

A 6-story RC building with base isolation using rubber bearings and viscous dampers has been recently built in Shanghai. Since the building is founded on soft soil, concern regarding base isolation suitability arose; even the Chinese design code does not recommend this solution for soft soil. To clarify this issue, nonlinear time-history analyses are carried out for a number of natural and artificial seismic inputs that represent the site seismicity, accounting for the soil conditions. The relevance of soil-structure interaction is discussed and some simulations are performed. Adequacy of base isolation is assessed both in the superstructure and the isolation layer. In the superstructure, appropriateness is judged in terms of reduction of interstory drift, absolute acceleration and shear force. In isolators, correctness is evaluated in terms of axial force, torsion angle and lateral displacement; prescriptions of Chinese and European regulations are considered. The major conclusion is that base isolation of ordinary mid-height RC buildings founded on soft soil can perform satisfactorily in medium seismicity regions.

Keywords: RC Building; Base Isolation; Rubber Bearing; Soft Soil; Nonlinear Dynamic Analysis

1. Introduction

A 6-story RC (reinforced concrete) building with rubber isolator units and viscous dampers has been recently constructed in Shanghai [Weng et al. 2012]. The building had been designed for seismic intensity degree 7 according to the current Chinese code [GB50011 2010], whose input peak accelerations are 0.10 and 0.22 g for moderate and rare earthquakes, respectively. The building is founded on soft soil; it is widely accepted that base isolation is less efficient for soft soil and even the Chinese code [GB50011 2010] does not recommend this solution for that soil condition. Therefore, concern regarding suitability of base isolation developed. Main reason for this prevention is that soft soil filters out the short period waves while amplifies the long period components; therefore, given the similarity between long periods of input and those of isolation system, in superstructure ground motion could prove enlarged, instead of reduced. Several previous studies on this subject have been published [Constantinou, Kneifati 1988; Spirakos et al. 2009a, 2009b; Enomoto et al. 2012; Alavi, Alidoost 2012]. To clarify this issue, seismic performance of base-isolated building is evaluated through nonlinear time-history analyses for a number of seismic inputs. These accelerograms are selected to represent the site seismicity, mainly accounting for soil conditions. Need for considering soil-structure interaction (SSI) is discussed, and numerical simulations are carried out.

Adequacy of base isolation is assessed in both the superstructure and the isolation layer. In the superstructure, appropriateness of base isolation is judged in terms of reduction of interstory drift, absolute acceleration and shear force. In isolators, correctness is evaluated in terms of axial force, torsion angle and lateral displacement (shear strain); for this purpose, prescriptions of the Chinese code [GB50011 2010] and the European regulations for base isolation [EN 1998-1 2004, EN 15129 2009] and for rubber bearings [EN 1337-3 2005] are considered.

2. Building under consideration

The structure of the analyzed building is a RC frame; there are no shear walls or other structural or non-structural members that might provide significant lateral stiffening or strengthening effect. The building has six stories and one basement; isolators are placed at ground level, i.e. on top of basement columns. Fig. 1 represents the analyzed building; Fig. 1.a displays a 3-D rendered view and Fig. 1.b represents the structural configuration, indicating columns (black squares) and beams.

Fig. 1 shows that the plan area is rectangular and the configuration is essentially regular; width, depth and height are 58.5 m, 18.3 m and 22.95 m, respectively. Columns have constant rectangular cross section ranging between 60 cm × 70 cm (inner columns) and 90 cm × 90 cm (corner columns). Slabs are formed by rectangular beams that are 30 to 35 cm wide and 50 to 70 cm deep; slabs are 11 to 14 cm deep. The characteristic value of the concrete compressive strength is f_{ck} = 30 MPa and the deformation modulus is estimated as E_{c} = 30 GPa. Reference [Weng et al. 2012] contains deeper information on the structural parameters. Live (variable) gravity loads are established according to the Chinese design code [GB50009 2012], ranging between 2 and 2.5 kN/m^2, except for stairs and other highly crowded areas. Seismic weight corresponds to combination D + 0.5 L, where D and L account for dead (permanent) and live (variable) loads, respectively. For this loading level, the building mass is 9576 t; from first to top (6$^{\text{th}}$) stories, floor masses are 1569, 1652, 1607, 1621, 1854 and 1273 t, respectively. To verify the influence of irregular arrangements of columns and other unevenness (e.g. balconies) in the structural symmetry, eccentricities between mass and rigidity centers of each floor are determined. In x direction, eccentricity ranges between 0.15% (first floor) and 0.70% (top floor) while in y direction, it ranges

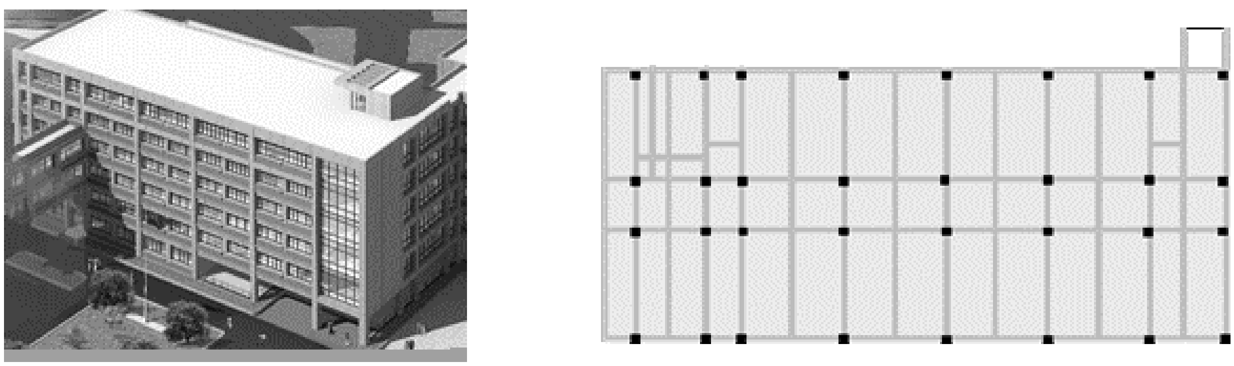

(a) 3-D representation (b) Plan layout

Fig. 1 – Analyzed building

between 3.75% (top floor) and 5.14% (first floor).

Table 1. Rubber bearings

Name	Diameter (mm)	Height (mm)	Rubber layer height (mm)	Rubber height (mm)	Lead plug diameter (mm)	Horizontal stiffness (kN/m)	Critical shear strain / stress (% / MPa)	Yielding force (kN)	After-yielding horizontal stiffness (kN/m)
NRB700	700	451.5	5	200	-	742	280 / 8	-	-
NRB800	800	438.5	6	204	-	951	301 / 10	-	-
LRB700	700	451.5	5	200	160	1565	282 / 8	160	764
LRB800	800	438.5	6	204	160	1758	304 / 10	160	972

The isolation system is formed by the parallel combination of rubber bearings [FUYO Tech 2010] and viscous dampers. Two types of rubber isolator units are employed: ordinary natural rubber bearings and lead-rubber bearings, i.e. incorporating a central lead plug core to provide additional damping. Those devices are termed along this paper NRB and LRB, respectively. The shear modulus of rubber is G = 0.392 N/mm^2. Apart from this common value, Table 1 displays the main geometric and mechanic characteristics of rubber isolators. Two types of viscous dampers are employed, being installed in x and y directions, respectively. Table 2 displays the major characteristics of those devices; Section 4 provides information relevant to the meaning of these parameters.

Table 2. Viscous dampers

Direction	**Exponent α**	**Initial stiffness (kN/mm)**	**Maximum stroke (mm)**	**Damping coefficient *c* (kN/(mm/s)$^{0.4}$)**	**Speed (mm/s)**	**Maximum damping force (kN)**	**Design life (Years)**
x	0.4	49	± 350	70	600	900	50
y	0.4	42	± 350	60	600	800	50

Fig. 2 displays the plan layout of isolators and dampers. Fig. 2 shows that isolators and dampers are arranged symmetrically; as well, dampers and bearings with lead plugs are located near the building perimeter, thus providing high torsional damping.

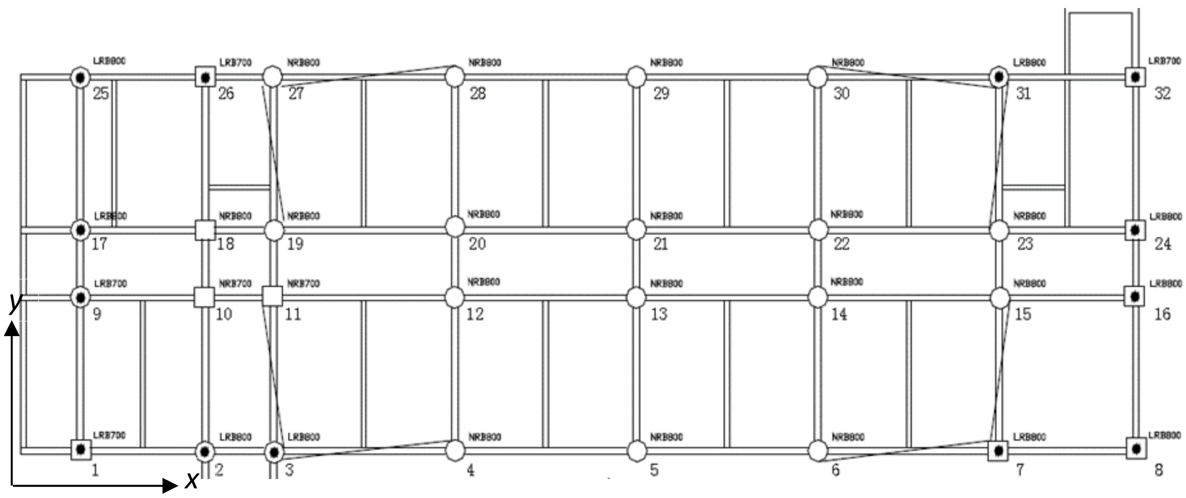

○,□: Natural rubber bearings ⊙,▣: Lead-rubber bearings : Viscous damper

Fig. 2 – Installation of isolators and dampers in the building

Since the soil is soft, the building is founded on piles. Each pile has 600 mm diameter and is 28 m deep. Bedrock in Shanghai is often located 200 ~ 300 m underground, being covered by thick quaternary unconsolidated sediments. For categorization purposes, the soil is divided into 9 layers, and each layer is split into several sub-layers. At bottom piles depth (28 m), soil condition is classified as layer 7-1, "grey clay silt"; average shear wave velocity down to 30 m (v_{s30}) ranges between 84 and 256 m/s [DGJ 08-37 2012]. For seismic design, the soil is categorized as type IV; this is the softest class, according to the Chinese code [GB50011 2010]. Section 3 discusses more deeply the ground parameters that are relevant to soil-structure interaction.

3. Numerical modeling of the dynamic behavior of the isolated building

Building lateral dynamic behavior is described with a linear 3D model. Beams and columns are represented by frame elements and slabs are modeled with shell elements. The rigid diaphragm effect of slabs is indirectly considered by its high in-plane stiffness. The stiffness of members is based on gross sectional parameters reduced to account for cracking; the reducing coefficient is 0.5 for beams and 1 for columns and slabs [FEMA 356 2000]. Noticeably, that reduction is unnecessary in the Chinese code [GB50011 2010]. Damping is described by a classical Rayleigh model whose mass and stiffness coefficients are selected for damping factor 0.05 in the first two modes.

The behavior of natural and lead-rubber bearings is described by a linear and by a classical hysteretic bilinear model, respectively. Table 1 displays the main parameters of both models. The torsional stiffness of the rubber bearings is neglected. The behavior of dampers is represented by a nonlinear viscous damping model:

$$f = c\,\dot{x}^{\alpha} \qquad (1)$$

The values of the damping coefficient c and the exponent α in equation (1) are listed in Table 2.

A number of studies on the relevance of soil-structure interaction (SSI) in base-isolated structures have been reported. Early work [Constantinou, Kneifati 1988] concluded broadly that SSI is less important in base-isolated than in fixed-base structures. More recently, some studies [Spyrakos et al. 2009a, 2009b] deduced that the SSI importance on the system damping is relatively small and that the SSI effects might be significant for relatively stiff and squat structures. In recent dates, paper [Alavi, Alidoost 2012] shows that SSI increases the fundamental periods of base-isolated buildings on different soil types and with different heights; the rate of increase is significant for structures on soft soil, being negligible for stiff soil. As a summary, all the previous studies conclude that the consideration of SSI is not necessary unless the soil is highly soft and the building is relatively stiff. Moreover, SSI is rather beneficial. The above studies seem to indicate that, given the high lateral flexibility of the isolated building, SSI might be neglected. However, just for additional safety, a simplified SSI study is performed. The SSI analysis is carried out using 3D uncoupled linear spring model [FEMA 273 1997]. This model consists in representing the interaction by six springs connecting each pile cap to the adjoining soil. Two approaches are considered to calculate the axial stiffness of each pile: (i) piles are assumed laying on a rigid bedrock, and, therefore, their stiffness is $E_p\ A_p\ /\ L_p$, and (ii) since piles do not actually reach the bedrock, only friction stiffness is accounted for. In this case, the friction vertical stiffness K_{vf} of a pile can be calculated by the formulation proposed in [Gazetas and Makris 1991]:

$$K_{\mathrm{vf}} = 1.8\ E_{\mathrm{s}}\ D_{\mathrm{p}}\ \lambda^{0.55}\ \eta^{-b} \qquad (2)$$

In equation (2), E_s is the soil modulus of elasticity, D_p is the pile diameter, λ is the ratio between pile length and diameter ($\lambda = L_p / D_p$), η is the ratio between soil and pile modulus of elasticity ($\eta = E_p / E_s$), and the exponent b is given by $b = \lambda / \eta$. In this case, E_p = 26 GPa, L_p = 28 m, D_p = 0.60 m, and E_s is calculated after the shear modulus G_s based on the weighted average shear wave velocity (v_s) and density (ρ_s) on the top 28 m. Table 3 displays the soil properties at each layer in the top 28 m:

Table 3. Soil layer parameters

Layer type	Cumulated depth (m)	Density (kg/m^3)	Shear wave velocity (m/s)
Filled earth	4.2	1870	112
Muddy-silty clay	9.5	1820	128
Muddy clay	22.5	1760	178
Muddy-silty clay	32.8	1800	245

In this case, the average values are along the top 28 m are v_s =171.8 m/s and ρ_s =1795 kg/m^3; therefore: G_s =53 MPa, and, by assuming a Poisson ratio ν = 0.25, E_s =132.5 MPa. Finally, K_{vf} =337 593 KN/m. Comparison with $E_p\ A_p\ /\ L_p$ shows that the friction stiffness is 1.286 times higher, what is consistent with estimations in [ATC-40 1996]. For each cap, the vertical spring stiffness is obtained as the sum of the axial stiffness of each pile.

After vertical stiffness of each pile, rotational stiffness with respect to horizontal axes are determined by equilibrium equations. For each cap, torsional and horizontal stiffness are determined, in terms of soil parameters and foundation dimensions, and as indicated in [Gazetas 1991]. Soil damping effect is neglected; this is a conservative assumption, since it would decrease base shear force.

4. Modal analysis of the isolated building

Table 4. Modal parameters of the building under fixed-base / base-isolation conditions

Mode No.	Period (s)	Modal mass factor *x*	Modal mass factor *y*	Modal mass factor φ
– / 1	– / 3.586	– / 0.046	– / **0.910**	– / 0.03561
– / 2	– / 3.528	– / **0.940**	– / 0.053	– / 0.0039
– / 3	– / 2.983	– / 0.011	– / 0.029	– / **0.96049**
1 / 4	1.229 / 0.571	0.010 / 7.25E-07	**0.717** / 0.004	0.074 / 1.142
2 / 5	1.163 / 0.502	**0.621** / 2.29E-03	0.046 / 1.02E-06	0.156 / 2.23E-06
3 / 6	1.106 / 0.177	0.196 / 7.08E-08	0.037 / 0.39E-06	**0.569** / 8.59E-08

Linear modal analyses of the building under fixed-base and isolation conditions are carried out using the previously described models. Table 4 displays periods and modal mass ratios of first six modes of base-isolated building and of first three modes of fixed-base building; φ accounts for twist angle (torsion). Since the incorporation of the isolation layer adds three new modes, in Table 4 first three modes of the fixed-base building are associated with the 4th, 5th and 6th modes of the base-isolated building, respectively. In the isolated building, periods are calculated for the effective secant stiffness (of lead-rubber isolators) that correspond to 100% shear strain. The highlighted values correspond to the biggest component, in terms of modal mass factor, of each mode. Figures from Table 4 provide the following remarks:

- **Fixed-base building**. First mode corresponds basically to motion along *y* direction and to torsion, second mode involves motion along *x* direction and torsion, and third mode contains mainly torsion. The relatively long period of the third mode (1.106 s) indicates low torsional stiffness; this is coherent with the absence of any important stiffening element in the façades. Given that this period is rather long, further verifications are carried out. The simplified expression for regular reinforced concrete frames contained in European [EN 1998-1 2004] and American [UBC 1997] codes provides a fundamental period equal to 0.676 s; since the building is rather flexible (because base isolation allows for significant reductions in the lateral design forces), this difference is feasible.
- **Base-isolated building**. First three modes correspond basically to motion along *y*, *x* and φ directions, respectively. First three modes cover most of mass; this indicates a rather satisfactory performance of base isolation since those modes correspond basically to rigid-body motion, without any structural damage.
- **Fixed-base vs. base-isolated building**. Comparison among periods of first three modes of the base-isolated building and those of the fixed-base building, shows that base isolation elongates periods as expected. Similar comparison among modal mass factors, shows that the base-isolated building behaves more symmetrically; this can be read as a proper design of the isolation system.

Table 5. Modal parameters of the base-isolated building with and without SSI

Mode No.	Period (s)			Modal mass factor *x*			Modal mass factor *y*			Modal mass factor φ		
	SSI-a	**SSI-b**	**No SSI**	**SSI-a**	**SSI-b**	**No SSI**	**SSI-a**	**SSI-b**	**No SSI**	**SSI-a**	**SSI-b**	**No SSI**
1	3.603	3.608	3.586	0.032	0.053	0.046	**0.942**	**0.877**	**0.910**	0.023	0.067	0.036
2	3.544	3.540	3.528	**0.957**	**0.922**	**0.940**	0.036	0.067	0.053	0.004	0.008	0.004
3	2.892	3.178	2.983	0.008	0.022	0.011	0.018	0.052	0.029	**0.972**	**0.921**	**0.961**
4	0.443	0.661	0.571	0.002	–	–	–	0.003	0.004	–	–	–
5	0.306	0.600	0.502	–	0.002	–	0.004	–	–	0.001	0.001	–
6	0.193	0.580	0.177	–	0.001	–	–	–	–	–	0.003	–

Table 5 displays periods and modal mass ratios of the the first six modes of the base-isolated building by considering and neglecting SSI; values of mass ratio that are smaller than 10^{-3} are indicated as "–". In Table 5, SSI-a and SSI-b correspond to axial and friction stiffness of piles, respectively. As in Table 4, highlighted values correspond to the biggest component, in terms of modal mass factor, of each mode. Figures from Table 5 show that the influence of SSI on periods and modal mass ratios of the first three modes can be ignored. Comparison between both models of SSI shows little influence of the vertical stiffness of piles; therefore, SSI results are reliable.

5. Seismic inputs

Representative accelerograms are selected according to former and current Shanghai design codes [DGJ 08-9 2003, 2013]. Two sets of seven trios of accelerograms (in two horizontal directions and in vertical direction) are chosen. Each set is composed of five natural earthquake records and two artificial inputs. Records are taken from PEER [PEER 2011] and artificial inputs are created by modifying historic accelerograms. First set corresponds to soil with predominant period 0.9 s and are scaled to maximum acceleration 1 m/s^2 (moderate earthquake); for second set, soil period is 1.1 s and maximum acceleration is 2.2 m/s^2 (rare earthquake). Table 6 and Table 7 display major features of both sets, respectively. In left column, "NR" accounts for "Natural Record" while "AW" means "Artificial Wave". *x* / *y* directions correspond to strong / weak components, respectively. I_{A} is Arias Intensity [Arias 1970] given by $I_{\mathrm{A}} = \frac{\pi}{2\,g} \int \ddot{x}_{\mathrm{g}}^2 \, dt$, where $\ddot{x}_{\mathrm{g}}$ is the input ground acceleration; Arias intensity is an estimator of the input severity. I_{D} is the dimensionless seismic index [Manfredi 2001] given by $I_{\mathrm{D}} = \frac{\int \ddot{x}_{\mathrm{g}}^2 \, dt}{PGA\;PGV}$. I_{D} accounts for the relevance of velocity pulses. Trifunac duration is the elapsed time between 5% and

95% of Arias Intensity I_A [Trifunac, Brady 1975]. Closest distance corresponds to the shortest way to the rupture surface. Hypocentral distance is the straight separation between the hypocentre and the recording station. v_{s30} is the weighted average shear wave velocity in the top 30 m; this parameter characterizes the soil type.

Table 6. Seismic inputs for soil predominant period 0.9 s and scaled to maximum acceleration 1 m/s^2

Code	**EQ**	**Date**	M_w	**Hypocentre depth (km)**	**Station**	**Component**		**PGV (m/s)**	**PGD (cm)**	I_A **(m/s)**	I_D	**Trifunac duration (s)**	**Closest distance (km)**	**Hypocentral distance (km)**	v_{s30} **(m/s)**
NR0.9-3	Kocaeli, Turkey	1999-08-17	7.51	15.0	USAK	*x*	USK090	0.272	4.831	0.451	10.36	35.52	226.7	237.0	274.5
						y	USK180	0.310	7.700	0.264	5.32	35.36			
NR0.9-4	Hector Mine, USA	1999-10-16	7.13	5.0	San Bernardino Fire Station #9	*x*	0688c090	0.262	3.967	0.317	7.56	20.44	108.0	114.8	271.4
						y	0688a360	0.123	7.532	0.280	14.22	28.10			
NR0.9-5	Denali, USA	2002-11-03	7.9	4.9	Anchorage New Fire Station #7	*x*	1734090	0.262	3.967	0.499	11.89	31.72	275.9	296.55	274.5
						y	1734360	0.228	2.060	0.561	15.37	29.80			
NR0.9-6	Chichi, Taiwan	1999-09-20	6.02	18.0	CHY039	*x*	CHY039-N	0.197	14.260	0.349	11.06	35.70	46.8	52.53	201.2
						y	CHY039-E	0.244	18.919	0.299	7.65	36.72			
NR0.9-7	Chichi, Taiwan	1999-09-20	7.62	18.0	CHY059	*x*	CHY059-N	0.185	14.162	0.398	13.44	38.56	86.3	88.53	191.1
						y	CHY059-E	0.190	6.717	0.361	11.87	33.94			
AW0.9-2	Loma Prieta, USA	1989-10-18	6.93	17.5	Foster City Menhaden Court	*x*	MEN270	0.272	2.138	0.317	7.28	22.08	45.4	68.0	126.4
						y	MEN360	0.242	2.211	0.308	7.95	20.10			
AW0.9-1	Hokkaido, Japan	2004-11-29	7.1	48	HKD085	*x*	HKD085EW	0.274	2.127	0.344	7.84	41.68	98.1	-	150.0
						y	HKD085NS	0.242	2.762	0.183	4.72	33.04			

Table 7. Seismic inputs for soil predominant period 1.1 s and scaled to maximum acceleration 2.2 m/s^2

Code	**EQ**	**Date**	M_w	**Hypocentre depth (km)**	**Station**	**Component**		**PGV (m/s)**	**PGD (cm)**	I_A **(m/s)**	I_D	**Trifunac duration (s)**	**Closest distance (km)**	**Hypocentral distance (km)**	v_{s30} **(m/s)**
NR1.1-3	Imperial Valley, USA	1979-10-15	7.62	10.0	El Centro Array #12	*x*	H-E12140	0.443	25.937	1.390	8.91	19.38	17.9	33.5	196.9
						y	H-E12230	0.284	20.607	0.975	9.75	19.14			
NR1.1-4	Chichi, Taiwan	1999-09-20	7.62	6.8	CHY058	*x*	CHY058-E	0.467	34.299	3.615	21.97	45.64	59.8	91.4	237.6
						y	CHY058-N	0.490	32.451	2.896	16.78	45.88			
NR1.1-5	Chichi, Taiwan	1999-09-20	7.62	6.8	CHY090	*x*	CHY090-E	0.446	28.146	2.917	18.57	38.78	58.4	89.8	201
						y	CHY090-N	0.556	40.618	2.569	13.12	45.32			
NR1.1-6	Chichi, Taiwan	1999-09-20	7.62	6.8	KAU008	*x*	KAU008-E	0.575	68.312	3.230	15.95	46.06	107.0	143.7	285.9
						y	KAU008-N	0.633	57.951	3.054	13.70	46.06			
NR1.1-7	Chichi, Taiwan	1999-09-20	7.62	6.8	KAU058	*x*	KAU058-E	0.584	76.979	3.172	15.42	40.16	107.8	143.3	201
						y	KAU058-N	0.717	72.504	4.263	16.88	46.84			
AW1.1-2	Morgan Hill	1984-04-24	6.19	8.5	Foster City APEEL 1	*x*	A01040	0.450	55.382	1.528	9.64	26.82	53.9	55.0	116.4
						y	A01310	0.552	50.816	1.558	8.01	26.56			
AW1.1-1	Hokkaido, Japan	2003-09-26	8.0	42	HKD066	*x*	HKD066EW	0.423	34.131	1.202	8.07	39.74	226.5	-	116.1
						y	HKD066NS	0.396	45.887	1.756	12.59	45.56			

The natural records are selected based on the similarity between their individual response spectra and the code design spectra. Figure 3 displays response spectra of natural selected inputs and code design spectrum. Noticeably, spectra in Figure 3 correspond to records scaled to 1 m/s^2; therefore, plots in Figure 3.c and Figure 3.d are reduced by factor of 2.2. Figure 3 show satisfactory fit between spectra of scaled inputs and code spectrum, particularly in main (*x*) direction. The artificial inputs are designed to fit the design spectrum, according to [GB50011 2010]. Fitting is established through 100 control points with logarithmic distribution in the interval [2 Δt, 10 s], where Δt = 0.02 s. Tolerance is 5%, in terms of quadratic error.

6. Time-history analysis

This section discusses results of time-history analyses for the inputs described in the previous section; *x* / *y* input components are applied on *x* / *y* directions (Fig. 2), respectively. The most meaningful results in superstructure are drift angle, shear force and absolute acceleration; in the isolators are also axial force, shear strain and torsion angle.

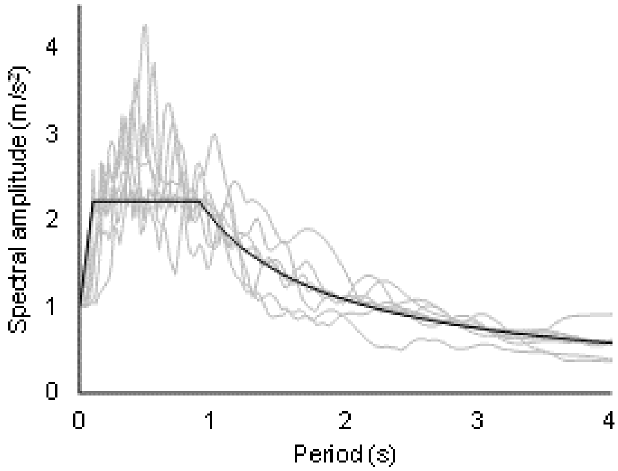

(a) Soil predominant period 0.9 s. *x* direction

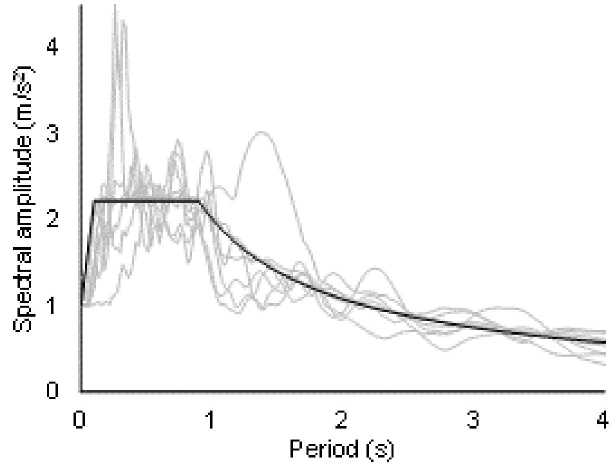

(b) Soil predominant period 0.9 s. *y* direction

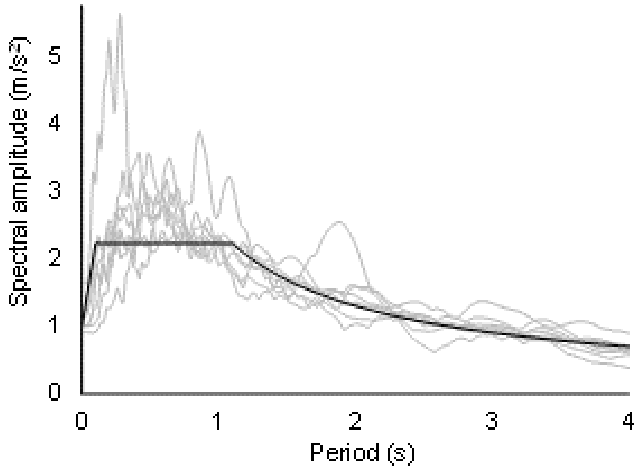

(c) Soil predominant period 1.1 s. *x* direction

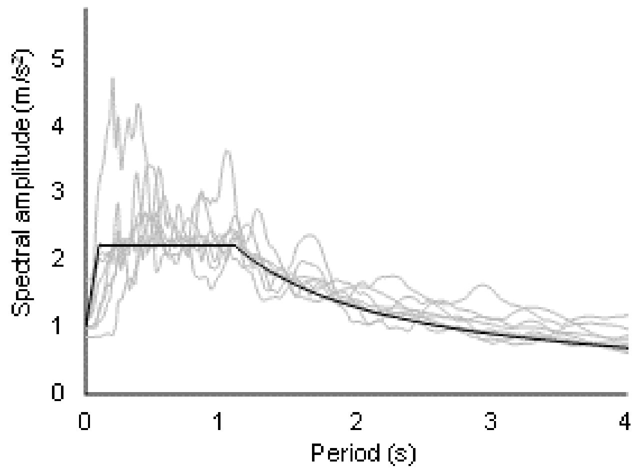

(d) Soil predominant period 1.1 s. *y* direction

Figure 3. Comparison between response spectra of natural selected inputs and code design spectra

The dynamic analyses are performed by implementing the numerical model described in section 3 in the SAP2000 v16.0 software package [Computers & Structures 2015]. The building behavior (superstructure) is linear, and nonlinearities are concentrated in the isolation layer. Analyses consider the simultaneous actuation of both horizontal input components. Time integration is performed by nonlinear modal analysis with $\Delta t = 0.02$ s. Analyses have not considered second order effects; it is observed that such effects in isolators do not over-magnify relative displacements, although can increase moments significantly, sometimes more than 10%.

Figure 4 displays sample representative time-history displacement responses and hysteresis loops of a natural rubber bearing (Figure 4.a and Figure 4.d), a lead-rubber bearing (Figure 4.b and Figure 4.e) and a viscous damper (Figure 4.c and Figure 4.f); labeling of isolator units and of damper corresponds to Fig. 2. All plots in Figure 4 correspond to input NR1.1-7 in *x* direction (Table 7). Figure 4 shows regular behavior. Similarity among time-history plots in Figure 4.a, Figure 4.b and Figure 4.c confirms the rigid diaphragm effect exerted by the ground floor slab. The hysteresis loops in Figure 4.d indicate linear behavior, without any encompassed area. Loops in Figure 4.d have almost rectangular shape, typical of plastification of metals. The shape of the hysteresis loops in Figure 4.f is closer to a rectangle than to an ellipse, this being consistent with the value of exponent α ($\alpha = 0.4$, Table 2).

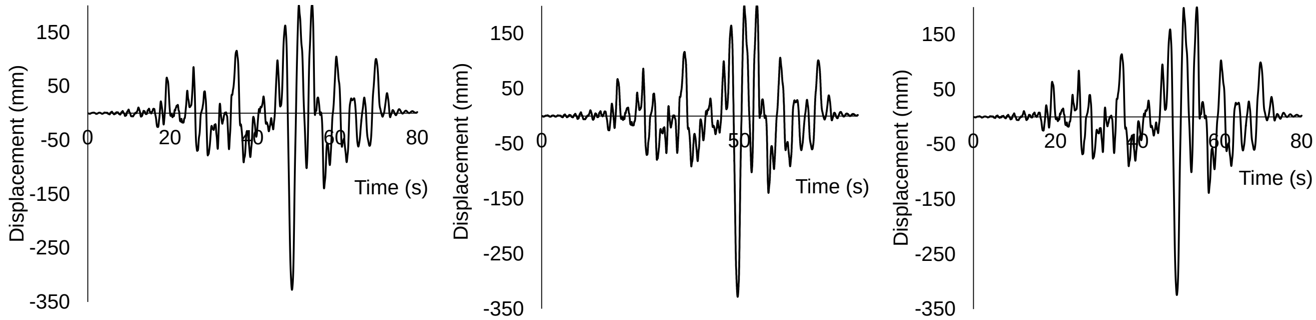

(a) NRB No. 27. Displacement time-history (b) LRB No. 32. Displacement time-history (c) Damper 27-28. Displacement time-history

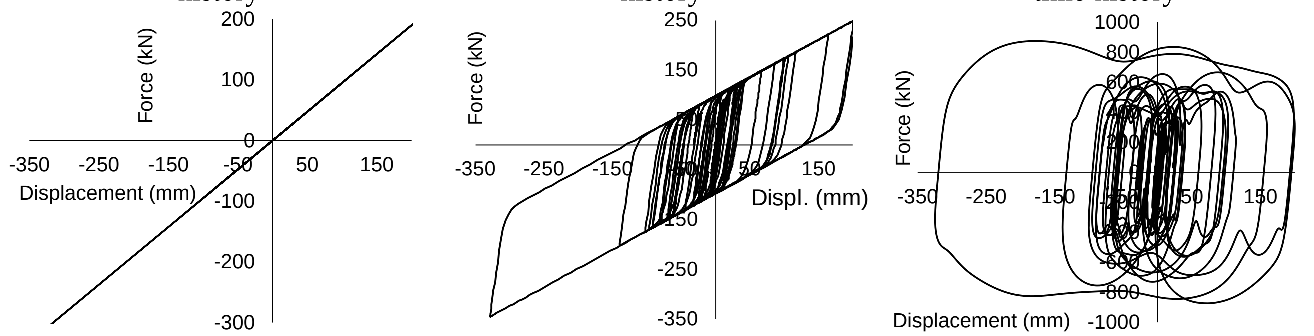

(d) NRB No. 27. Hysteresis loops (e) LRB No. 32. Hysteresis loops (f) Damper 27-28. Hysteresis loops

Figure 4. Dynamic responses of two isolators and a damper. Input NR1.1-7, x direction (Table 7)

Figure 5 depicts vertical profiles of drift angles (Figure 5.a and Figure 5.c) and absolute accelerations (Figure 5.b and Figure 5.d). Results in Figure 5 correspond to the average maximum values (during the input duration) of the inputs listed in Table 6 (Figure 5.a and Figure 5.b) and Table 7 (Figure 5.c and Figure 5.d). As indicated in the caption, plots in Figure 5 have been generated under the simultaneous actuation of two inputs in *x* and *y* directions; this situation is termed next as "*x* + *y*" in this paper.

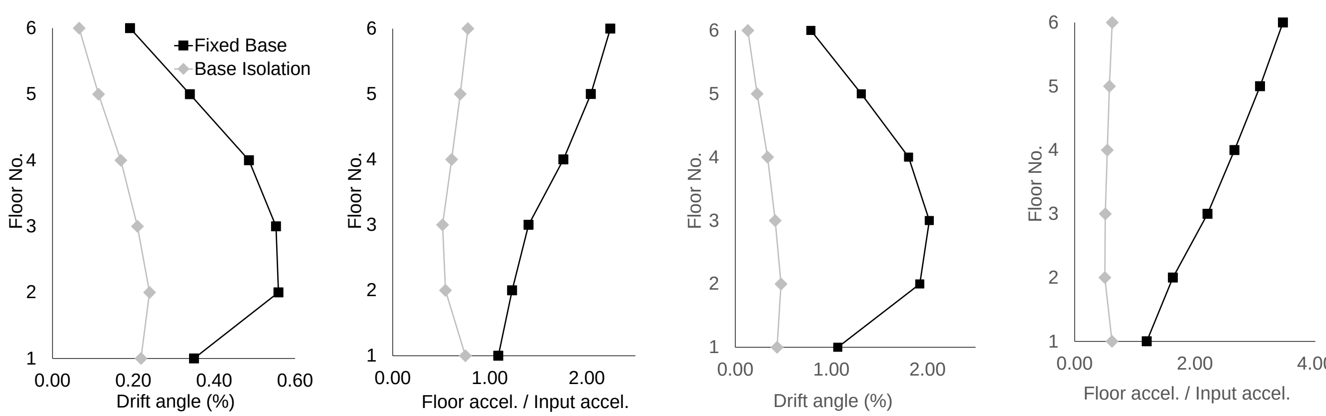

(a) Drift angle. Soil period 0.9 s

(b) Absolute acceleration / input acceleration. Soil period 0.9 s

(c) Drift angle. Soil period 1.1 s

(d) Absolute acceleration / input acceleration. Soil period 1.1 s

Figure 5. Vertical profiles of drift angles and absolute accelerations for combined *x* + *y* inputs

Table 8. Maximum and cumulated response values for selected inputs

Input			Maximum drift angle (%)		Maximum shear force / supported weight		Maximum acceleration / input acceleration		E_ζ / E_I (Structural Damping)	E_{HD} / E_I (Dampers)	E_{HI} / E_I (Isolators)
Code	Period (s)	Direction	Fixed-base	Base isolation	Fixed-base	Base isolation	Fixed-base	Base isolation	Base isolation		
NR0.9-3	0.9	x	0.388	0.108	0.151	0.042	2.79	0.771	0.196	0.551	0.247
		y	0.293	0.169	0.099	0.057	1.707	0.886	0.176	0.507	0.312
		$x + y$	0.400	0.168	0.156	0.058	2.281	0.723	0.177	0.508	0.313
NR0.9-6	0.9	x	0.363	0.108	0.148	0.044	2.493	0.716	0.151	0.557	0.292
		y	0.416	0.137	0.133	0.049	2.457	0.799	0.165	0.509	0.326
		$x + y$	0.388	0.151	0.164	0.061	2.394	0.812	0.148	0.525	0.327
AW0.9-1	0.9	x	0.271	0.113	0.101	0.041	1.996	0.799	0.165	0.565	0.262
		y	0.296	0.157	0.114	0.050	1.813	0.809	0.192	0.519	0.285
		$x + y$	0.421	0.184	0.148	0.059	2.052	0.788	0.167	0.552	0.276
NR1.1-5	1.1	x	0.689	0.191	0.317	0.083	2.531	0.656	0.145	0.532	0.322
		y	1.299	0.308	0.391	0.104	3.422	0.66	0.156	0.491	0.351
		$x + y$	1.460	0.294	0.410	0.117	3.652	0.665	0.151	0.532	0.316
NR1.1-7	1.1	x	1.028	0.265	0.444	0.123	3.212	0.628	0.154	0.531	0.314
		y	1.451	0.359	0.432	0.131	4.032	0.740	0.190	0.489	0.315
		$x + y$	1.632	0.332	0.444	0.154	4.166	0.782	0.176	0.527	0.297
AW1.1-1	1.1	x	0.716	0.174	0.301	0.079	2.457	0.528	0.138	0.533	0.328
		y	0.980	0.359	0.294	0.080	2.843	0.492	0.144	0.488	0.366
		$x + y$	1.280	0.282	0.410	0.106	2.571	0.428	0.137	0.519	0.342

Table 8 displays maximum drift angle, shear force and absolute acceleration for some inputs in Table 6 and Table 7. Figures in Table 8 are maximum along the building height (1st to 6th stories) and during the input duration. Shear force and absolute acceleration are normalized with respect to the supported weight and the maximum input acceleration, respectively. For the base-isolated building, Table 8 displays also ratios between the dissipated energies (E_ζ, E_{HD}, E_{HI}) and the input energy E_I. E_ζ is the energy dissipated by the structural damping, E_{HD} is the energy dissipated by the viscous dampers and E_{HI} is the energy dissipated by the rubber bearings; at the end of shake, energy balance equation reads $E_I \approx E_\zeta + E_{HD} + E_{HI}$. Figure 6 represents time-histories of energies E_I, E_ζ, E_{HD} and E_{HI} (Table 8) for input NR0.9-6 (Table 6). In Figure 6, "Input Energy", "Damping Energy", "Dampers Energy" and "Isolators Energy" account for E_I, E_ζ, E_{HD} and E_{HI}, respectively.

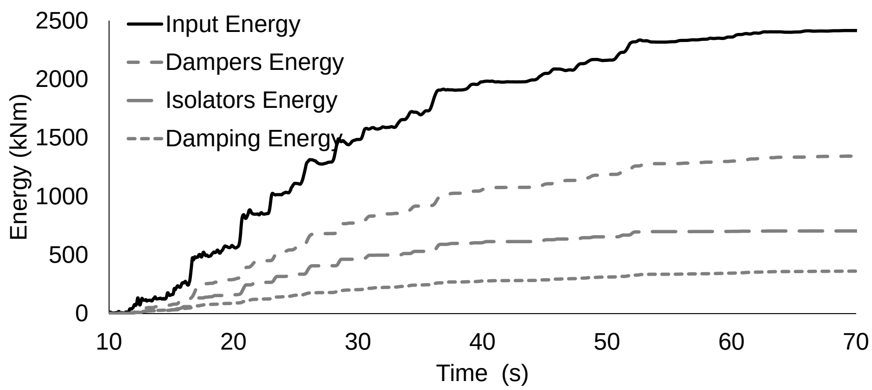

Figure 6. Time-history of energy balance for input NR0.9-6 (Table 6)

Table 8, Figure 5 and Figure 6 provide the following remarks:

- **Drift angle in superstructure**. Except in few cases, isolators reduce the drift displacements; lessening is lower in bottom stories. The rather moderate drift under isolation conditions for strong inputs, confirms that assuming linear behavior of superstructure is correct. In isolated building, drift angle is rather constant along first two stories and tends to decrease upwards. Comparison among results for inputs with maximum acceleration equal to 0.1 g and 0.22 g shows that reduction is higher for strongest inputs. This difference can be explained by nonlinear behavior of lead-rubber bearings: the higher the shear strain, the higher the equivalent damping and the lower the effective secant stiffness, thus leading to higher degree of isolation.

- **Drift angle in isolators**. Drift angle values for inputs with acceleration 0.22 g are more than 2.2 times higher than those for the inputs with 0.1 g. This implies nonlinear behavior of the lead-rubber bearings. However, no relevant permanent displacements are observed; this can be read as a satisfactory performance.
- **Shear coefficient in superstructure**. Isolation reduces significantly story shear forces; decreasing is higher for top stories and strongest inputs. For base-isolated building, shear coefficient is near constant along the building height.
- **Base shear coefficient**. Isolation reduces significantly base shear force. For the less strong inputs (Table 6), reduction ranges between 55% and 70%; for the strongest inputs (Table 7) reduction is roughly 75%. This difference can be explained by nonlinear behavior of lead-rubber bearings.
- **Absolute acceleration in superstructure**. Absolute acceleration at ground floor (right above the isolation layer) is not reduced, compared to the driving input. In other floors, absolute acceleration is reduced, compared to fixed-base case; reduction is higher in top stories. As well, such decreasing is more important for inputs with acceleration 0.22 g. Absolute acceleration is not uniform along building height. As expected, percentages of reduction of top floor absolute acceleration and base shear force are similar.
- **Dissipated energy**. Table 8 shows that percentage of energy dissipated by isolation interface is above 80%, being slightly higher for strong inputs. Comparison with ordinary values of ratio between input and hysteretic energies [López-Almansa et al. 2013] shows that is clearly above common demands. Plots from Figure 6 show that maximum values are obtained at end of shake. This confirms that using final values of energy is adequate.
- **Simultaneity of *x* and *y* inputs**. As expected, the average drift ratios and shear coefficients for simultaneous action of *x* and *y* inputs are bigger than those generated by *x* and *y* inputs acting separately. Conversely, regarding absolute acceleration, balance is unclear; this apparent inconsistency can be explained by building asymmetry, since any input generates responses with *x*, *y* and torsion (φ) components (Table 4).

To investigate the effect of SSI, Table 9 displays the base shear coefficient for inputs in Table 8. Three situations are considered: fixed-base without SSI, base isolation with SSI, and base isolation without SSI. SSI-a and SSI-b has same meaning than in Table 5. Comparison between last two columns in Table 9 shows that effect of SSI is only moderate. Therefore, it can be globally concluded that SSI does not play a leading role. Results for both SSI models are similar, thus showing little influence of the vertical stiffness of piles.

Table 9. Base shear coefficient with and without SSI

Input			Base shear force / Building weight		
Code	**Period (s)**	**Direction**	**Fixed-base without SSI**	**Base isolation with SSI-a / SSI-b**	**Base isolation without SSI**
NR0.9-3	0.9	*x*	0.148	0.041 / 0.042	0.041
		y	0.097	0.044 / 0.060	0.056
NR0.9-6	0.9	*x*	0.145	0.043 / 0.044	0.043
		y	0.131	0.032 / 0.048	0.048
AW0.9-1	0.9	*x*	0.099	0.044 / 0.042	0.041
		y	0.112	0.035 / 0.048	0.049
NR1.1-5	1.1	*x*	0.311	0.085 / 0.086	0.081
		y	0.384	0.097 / 0.100	0.102
NR1.1-7	1.1	*x*	0.436	0.123 / 0.120	0.121
		y	0.423	0.134 / 0.126	0.128
AW1.1-1	1.1	*x*	0.295	0.079 / 0.081	0.078
		y	0.290	0.072 / 0.080	0.079

The performance of the rubber isolators in terms of buckling instability and shear deformation is discussed next. Table 10 shows, for isolators No. 29, 32, 24 and 17 (Fig. 2), maximum values of axial force, torsion angle and drift displacement. Displayed figures correspond to seismic inputs in Table 8; axial force generated by gravity loads (combination D + 0.5 L) is also shown (bottom row). Similarly to Table 8, "*x*", "*y*" and "*x* + *y*" inputs are presented; herein, moreover results corresponding to combination of responses in *x* and *y* directions are also shown. These combinations are obtained [EN 1998-1 2004] by two empirical criteria: SRSS (Square Root of

Sum of Squares) and $X + 0.3Y$ or $Y + 0.3X$ where X and Y represent effect of inputs in x and y directions, respectively. For axial force and torsion angle, combinations are $\sqrt{X^2+Y^2}$ and $X + 0.3Y$ or $Y + 0.3X$, and for drift displacements are $\sqrt{X^2+(0.3Y)^2}$ and $\sqrt{(0.3X)^2+Y^2}$. Comparison among cases "Combination" and "$x + y$" shows low correlation. Therefore, usual empirical combination criteria are not always on safe side.

Table 10. Maximum response values for isolators No. 29 (NRB), 32 (LRB), 24 (LRB) and 17 (LRB)

Input			**Axial force (kN)**				**Torsion angle (rad)**	**Drift displacement (mm)**
Code	**Period (s)**	**Input direction**	**No. 32**	**No. 24**	**No. 29**	**No. 17**		
NR0.9-3	0.9	x	338.1	266.5	12.7	409	0.00129	44
		y	467.8	921.5	430.3	789.1	0.00176	104
		Combination	577.2	1001.5	434.1	911.8	0.00180	105
		$x + y$	645.5	1010.9	424.7	713.9	0.00175	103
NR0.9-6	0.9	x	361.2	284.4	13.8	408.2	0.00129	46
		y	370.2	738	342.3	630.7	0.00143	76
		Combination	517.2	823.3	346.4	753.2	0.00143	77
		$x + y$	681.8	935.1	294.6	527.3	0.00127	89
AW0.9-1	0.9	x	398.6	315.7	10.5	343.9	0.00136	42
		y	246.5	484.8	226.9	415	0.00164	76
		Combination	472.6	579.5	230.1	539.0	0.00164	77
		$x + y$	298.4	397.5	218.3	567.1	0.00161	86
NR1.1-5	1.1	x	594	466.9	22.3	717.4	0.00229	186
		y	839.7	1669.2	772.3	1435.4	0.00321	255
		Combination	1028.6	1809.3	779.0	1650.6	0.00320	261
		$x + y$	1188.6	1849.8	695.9	1367.8	0.00290	272
NR1.1-7	1.1	x	712.7	564.7	24.4	959.2	0.00317	329
		y	967.5	1938.1	882.6	1661.5	0.00375	355
		Combination	1201.7	2107.5	889.9	1949.3	0.00375	369
		$x + y$	1013.6	1971.3	918.5	2368.8	0.00391	491
AW1.1-1	1.1	x	606.9	477.3	15.6	543	0.00208	163
		y	499.7	990.7	458.5	849	0.00258	182
		Combination	786.1	1133.9	463.2	1011.9	0.00258	189
		$x + y$	624	1052	449.2	1309.5	0.00237	247
$D + 0.5\,L$	-	Vertical	2755.4	2565	4349	3730	-	-

Figures in Table 10 are used next to check requirements of Chinese code [GB50011 2010] and European regulation [EN 15129 2009] (8.2.3.4) in terms of buckling instability and maximum shear strain.

Buckling stability. [GB50011 2010] indicates that average drift displacement ≤ 0.55 × rubber diameter. This condition is fulfilled except in one case ("$x + y$"). This code does not require to consider that coincident actuation; for this unclear situation, European regulation [EN 15129 2009] is considered. In that code, critical load is given by $P_{cr} = \lambda\ G\ A_r\ a'\ S\ /\ T_q$ where $\lambda = 1.1$ (for circular devices), G is rubber shear deformation modulus, A_r is rubber bearing plan area, a' is device diameter, S is shape factor (ratio between device diameter and thickness of each rubber layer) and T_q is total rubber thickness. By neglecting stiffening effect of lead plug, critical loads are, for 700/800 mm diameter, $P_{cr} = 2.10 \times 10^4$ / 2.80×10^4 kN . Table 10 shows that maximum axial force in 700 mm isolators is $N_{Ed,max} = 4536$ kN (device # 24, input NR1.1-7, case "$x + y$") and in 800 mm isolators is $N_{Ed,max} = 6099$ kN (device # 17, input NR1.1-7, case "$x + y$"); thus, in both cases $N_{Ed,max} < P_{cr} / 4$. According to EN 1337-3, it should be checked that $\delta \leq 0.7$ where δ is ratio between design drift displacement d_{bd} and device diameter. Design drift is conservatively taken as maximum value in Table 10: $\delta = 491 / 700 = 0.7$ and $\delta = 491 / 800 = 0.61$ for 700 and 800 mm isolators, respectively. Therefore, criterion is fulfilled for both types of devices.

Maximum shear strain. In EN1337-3, maximum shear strain is given by $\varepsilon_{t,d} = K_L\ (\varepsilon_{c,E} + \varepsilon_{q,max} + \varepsilon_{\alpha,d})$ where $K_L = 1$, $\varepsilon_{c,E} = 6\ S\ /\ A_r\ E'_c$, $E'_c = 3\ G\ (1 + 2\ S^2)$, $\varepsilon_{q,max} = d_{bd}\ /\ T_q \leq 2.5$, and $\varepsilon_{\alpha,d} = (a'^2\ \alpha_{ad} + b'^2\ \alpha_{bd})\ t_r\ /\ 2\ \Sigma\ t^3_r$ where $\alpha_{ad} = \alpha_{bd} = 0.003$, $a' = b'$ (for circular devices), and t_r is thickness of each rubber layer. For 700/800 mm diameter isolators E'_c = 2882/2614 MPa. Then, for 700/800 mm diameter, $\varepsilon_{t,d} = 4.77/4.90$. Since both results are smaller than 7 / γ_m (where γ_m is a safety factor, being γ_m = 1), criterion is fulfilled.

7. Conclusions

This paper investigates the suitability of rubber bearing isolation of a 6-story RC building in Shanghai that is founded on soft soil. The verification consists in performing nonlinear time-history analyses for seismic inputs selected to represent the site seismicity, given the soil conditions. Two sets of seven inputs each are considered; in the first/second set inputs the maximum acceleration is 0.1/0.22 g. A simplified uncoupled linear model represents soil-structure interaction. The overall conclusion of this study is that isolation performs satisfactorily, both in terms of demand on isolation system and input on superstructure. This research shows that base isolation, if properly designed and implemented, can be an efficient solution for ordinary mid-height RC buildings founded on soft soil and located in medium seismicity regions, like Shanghai.

8. Acknowledgements

This work is supported Spanish Government, projects BIA2014-60093-R and CGL2015-6591. The stay of Mr. Li in Barcelona was funded by College of Civil Engineering of Tongji University.

9. References

[1] Alavi E, Alidoost M (2012): Soil-Structure Interaction Effects on Seismic Behavior of Base-Isolated Buildings. *15WCEE*.
[2] Arias A (1970): *A measure of earthquake intensity. Seismic Design for Nuclear Power Plants*. MIT Press 438-443.
[3] ATC-40. (1996): *Seismic evaluation and retrofit of concrete buildings*. Applied Technology Council.
[4] Constantinou M, Kneifati M (1988): Dynamics of Soil-Base-Isolated-Structure Systems. *Journal of Structural Engineering ASCE*, 114(1), 211–221.
[5] Computers & Structures Inc. (2015): CSI Analysis Reference Manual for SAP2000®, ETABS®, and SAFE™, available from www.comp-engineering.com.
[6] DGJ 08-9 (2003): *Code for Seismic Design of Buildings. Shanghai Construction and Management Commission*.
[7] DGJ 08-9 (2013): *Code for Seismic Design of Buildings. Tongji University Shanghai Urban Construction and Communication Commission*.
[8] DGJ 08-37 (2012): *Code for Investigation of Geotechnical Engineering*. Shanghai Geotechnical Inv. & Design Institute.
[9] EN 1337-3 (2005): *Structural bearings. Part 3: Elastomeric bearings*. European committee for standardization.
[10] EN 15129 (2009): *Anti-seismic devices.* European committee for standardization.
[11] EN 1998-1 (2004): *Eurocode 8: Design of structures for earthquake resistance*. European committee for standardization.
[12] Enomoto T, Yamamoto T, Ninomiya M, Miyamoto Y, Navarro M (2012): Seismic Response Analysis of Base Isolated RC Building Building Considering Dynamical Interaction Between Soil and Structure. *15WCEE*. Lisbon. Paper No. 3611.
[13] FEMA 273 (1997): *NEHRP Guidelines for the Seismic Rehabilitation of Buildings*. FEMA.
[14] FEMA 356 (2000): *Prestandard and commentary for the seismic rehabilitation of buildings*. FEMA.
[15] FUYO Tech (2010): *Lead Rubber Bearings and Rubber Bearings (G4)*. Wuxi FUYO Tech Co., Ltd. http://www.fuyotech.com.
[16] Gazetas G (1991): Formulas and charts for impedances of surface and embedded foundations. Journal of Geotechnical Engineering ASCE.117(9):1363–81.
[17] Gazetas G, Makris N (1991): Dynamic pile-soil-pile interaction. *Ethqk. Eng. & Structural Dynamics*. 20:115-132.
[18] GB50010 (2010): *Code for Design of Concrete Structures*. Ministry of Housing and Urban-Rural Development. China.
[19] GB50011 (2010): *Code for Seismic Design of Buildings*. Ministry of Housing and Urban-Rural Development. China.
[20] GB50009 (2012): *Load code for design of building structures*. Min. of Housing and Urban-Rural Development. China.
[21] López Almansa F, Yazgan U, Benavent Climent A (2013): Design energy input spectra for moderate-to-high seismicity regions based on Turkish registers. *Bulletin of Earthquake Eng*. 11(4) 885–912.
[22] Manfredi G (2001): Evaluation of seismic energy demand. *Earthquake Eng. & Structural Dynamics*, 30:485–499.
[23] PEER (2011): *User's manual for the PEER ground motion database web application*. Technical report, PEER.
[24] Spyrakos CC, Koutromanos IA, Maniatakis ChA (2009a): Seismic response of base-isolated buildings including soil–

structure interaction. *Soil Dynamics and Earthquake Engineering* 29:658–668.

[25] Spyrakos CC, Maniatakis ChA, Koutromanos IA (2009b): Soil-structure interaction effects on base-isolated buildings founded on soil stratum. *Engineering Structures* 31:729-737.

[26] Trifunac MD, Brady AG. (1975): Study on the duration of strong earthquake ground motion. *Bull. Seism.* 65:581–626.

[27] UBC (1997): *Uniform Building Code*, International Council of Building Officials.

[28] Weng D, Zhang S, Hu X, Chen T, Zhou Y (2012): *Seismic isolation design soil of a teaching building for Shanghai foreign language school* (in Chinese). Research Inst. of Struct. Eng. and Disaster Reduction, Tongji Univ., Shanghai.